Journal of Holistic Integrative Pharmacy 4 (2023) 281–286

Contents lists available at ScienceDirect

Journal of Holistic Integrative Pharmacy

journal homepage: www.keaipublishing.com/en/journals/journal-of-holistic-integrative-pharmacy

Synthesis, cytotoxicity study of novel bisacridine derivatives and their interaction with *c-myc* promoter G-quadruplex/i-motif

Bing Shu [a,*], Wang-liang Chen [a], Jia-lin Song [b], Shen Fang [a], Jiong-bang Li [a], Shang-shi Zhang [b,**]

[a] School of Pharmacy, Guangdong Pharmaceutical University, Guangzhou, 510006, China
[b] Center for Drug Research and Development, Guangdong Pharmaceutical University, Guangzhou, 510006, China

ARTICLE INFO

Keywords:
Synthesis
Bisacridine derivatives
G-quadruplex
I-motif
Cytotoxicity

ABSTRACT

Objective: To synthesize novel bisacridine derivatives **A1**-**A4** and study cytotoxicity and their interaction with *c-myc* G-quadruplex/i-motif DNA.
Method: Bisacridines **A1**-**A4** were synthesized according to the conventional reaction method. Fluorescence resonance energy transfer (FRET) melting assay, Surface Plasmon Resonance (SPR) measurement, CD experiments, and molecular docking were used to study the interactions between **A1**-**A4** and *c-myc* promoter G-quadruplex/i-motif. MTT cytotoxicity assay was used to evaluate the cytotoxicity of the bisacridine derivatives **A1**-**A4** against A375, Hela, A549, U2OS, HCT116, Siha, HuH7 cell lines.
Result: The results of FRET melting assay and SPR measurement indicated that bisacridine derivatives **A1**-**A4** could bind to and stabilize the *c-myc* G-quadruplex/i-motif structure. CD experiments and molecular docking results demonstrated the interaction between **A1**-**A4** and *c-myc* G-quadruplex/i-motif. MTT experiments showed that **A1**-**A4** exhibited strong inhibitory effects on the proliferation of human A375, Hela, A549, U2OS, HCT116, Siha, HuH7 cell lines.
Conclusion: Bisacridine derivatives **A1**-**A4** could bind to and stabilize the *c-myc* G-quadruplex/i-motif to inhibit the proliferation of human cancer cells and will potentially be developed into a class of small molecule ligands targeting *c-myc* G-quadruplex/i-motif.

1. Introduction

Cancer has become one of the most deadly diseases worldwide in the present society, with the incidence of the population being about 20 million cancer cases and mortality about 9.6 million deaths, according to WHO.[1,2] The human *c-myc* gene is an overexpression oncogene.[3–5] Aberrant overexpression of this gene is closely related to the occurrence and development of various human cancers.[6,7] Hence the up-regulation of *c-myc* is one of the hallmarks of many cancers.[8,9] The P1 promoter of *c-myc* gene is continuous guanine/cytosine-rich bases (GC-rich), which can open up to make the formation of two non-B-form unique DNA secondary structures: G-quadruplexe on the G-rich strand and i-motif on the complementary C-rich strand,[9,10] under physiological conditions.

G-quadruplexes are special DNA or RNA secondary structures, which are composed of consecutive guanine-rich sequences through Hoogsteen hydrogen bonds to form G-tetrads.[11,12] G-quadruplexes have been widely characterized to be more prevalent in cancer cells than non-neoplastic tissues by using the G-quadruplex antibody BG4 and are believed to play key roles as transcriptional repressors to modulate gene transcription of cancer cells.[13,14] The i-motifs comprise two parallel duplexes with intercalated hemiprotonated cytosine^{+}-cytosine (C^{+}-C) base pairs (also named C-quadruplexes).[15,16] Recent studies suggest the existence of i-motif structures in cells and their important roles in gene regulation to expected to be an attractive target for anticancer drug development and gene regulation processes[17,18] Several small molecules that can induce and stabilize these two quadruplex structures are, therefore, putative agents to down-regulate corresponding oncogene expression.[9,16,19,20]

Acridines are important nitrogen-containing heterocycle structural moieties with unique chemical properties that exist in both protonated and unprotonated forms, interacting with most nucleic acid multiplex structures, such as duplexs, or other bioactive molecules.[21] Mergny group has reported that a macrocycle containing two acridine subunits linked by two diethylenetriamine arms named **BisA** could increase the melting temperature of the G-quadruplex and i-motif at 1 μM dye concentration,

* Corresponding author.
** Corresponding author.
E-mail addresses: shubing@gdpu.edu.cn (B. Shu), zhangshangshi@gdpu.edu.cn (S.-s. Zhang).

https://doi.org/10.1016/j.jhip.2024.01.003
Received 19 December 2023; Received in revised form 19 January 2024; Accepted 19 January 2024

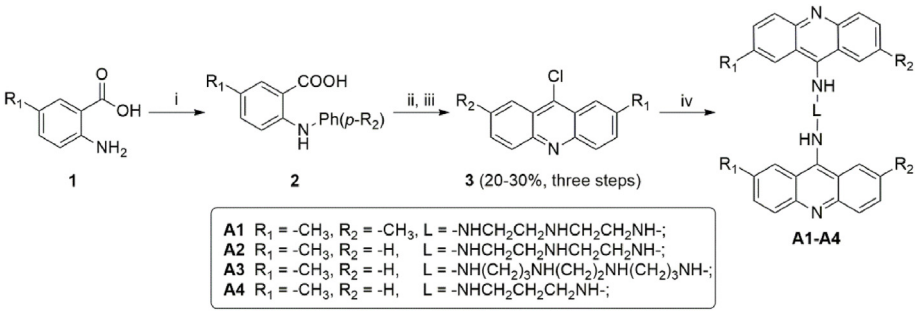

Fig. 1. The synthetic route of bisacridine derivatives (**A1-A4**). Reaction condition: (i) 1-Bromo-4-substituted benzene, Cu, CuI, K_2CO_3, dimethylformamide (DMF), 120 °C, 12 h; (ii) conc. H_2SO_4, 100 °C, 2 h; (iii) $POCl_3$, 100 °C, 3 h (20–30 % yield for three steps); (iv) NH_2-L-NH_2, PhOH, 100 °C, 8 h (yield 49–76 %).

much stronger than the **MonoA**, a monomeric acridine substituted by two propylaminomethyl groups.[22] In the previous research, we found that a monomeric acridine (named **AD06**) could stabilize *c-myc* G-quadruplex and i-motif structure with the ΔT_m value of 8.3 °C and 10.0 °C at 5 μM, respectively[1].[23] While **AD06** also displayed thermal stability to hairpin structure with $\Delta T_m = 6.8$ °C. In order to obtain much stronger G-quadruplex and i-motif binders and study the structure-activity relationship, we designed and synthesized a series of bisacridine derivatives (**A1-A4**) linked with various substitutive groups (Fig. 1). Subsequent experiments were applied to evaluate the interaction between bisacridine derivatives and *c-myc* G4/i-motif DNA such as fluorescence resonance energy transfer (FRET) melting point, surface plasmon resonance (SPR), circular dichroism (CD) titration experiment and molecular docking. Moreover, the anticancer activity effects of these acridine derivatives were also accomplished.

2. Experiments

2.1. Instruments and reagents

DF-101S thermostatic magnetic stirrer (Yuhua Instrument [Gongyi] Co., Ltd.); SHZ-D (III) circulating water multi-purpose vacuum pump (Henan Province Yuhua Instrument Co., Ltd.); Orion Model 720 A pH meter (Thermo Scientific, USA); Shimadzu LCMS-IT-TOF of MAT95XP mass spectrometer (Thermo Fisher Scientific, USA); NMR (Avance III 400 MHz, Bruker), Nano Drop 1000 Spectrophotometer (Thermo Fisher Scientific, USA); LightCycler 2 real-time PCR instrument (Roche, USA); ProteOn XPR36 Protein Interaction Array system (Bio-Rad Laboratories, Hercules, CA); Chirascan circular dichroism spectrophotometer (Applied Photophysics); Cell culture incubator (MCO-15AC, Sanyo); full wavelength enzyme-linked immunosorbent assay (PowerWave XS2, Biotek).

The commonly used chemical reagents are all domestically produced analytical grade without further treatment, purchased from Annaiji Chemical Reagent Co., Ltd, such as 2-amino-5-methylbenzoic acid, Cu, CuI, 1-bromo-4-substituted benzene, K_2CO_3, $POCl_3$, amines, dimethylformamide (DMF), PhOH and so on. FPu22T, FPy33T, F10T, Pu22, Py33, 5′-biotin Py33, 5′-biotin Pu22, and 5′-biotin duplex DNA used in this study were purchased from Sangon. Their concentrations were represented as single-stranded concentrations and determined from the absorbance at 260 nm with the Beer-Lambert Law: $A = \varepsilon \cdot C \cdot l$.

1 × BPES buffer (30 mM KH_2PO_4+K_2HPO_4, 1 mM EDTA, 100 mM KCl, pH 5.5), Tris-HCl buffer (10 mM KCl, 10 mM Tris-HCl, pH 7.4), Tris-HCl/KCl buffer (60 mM KCl, 10 mM Tris-HCl, pH 7.4), Py33 running buffer (20 mM 2-(4-morpholino)ethanesulfonic acid, pH 5.8, 100 mM KCl and 0.05 % Tween-20), Pu22/duplex running buffer (Tris-HCl 50 mM, 100 mM KCl, pH 7.4).

2.2. Synthetic route

Fig. 1 showed a synthetic pathway for bisacridine derivatives **A1-A4**. First, *o*-aminobenzoic acid **1** as starting materials reacted with bromobenzene through Cu catalyzed Ullmann reaction to afford intermediates **2** in a feature of crude mixture. Then **2** reacted in a solution of concentrated sulfuric acid to proceed crude acridone, subsequently reacted with phosphorus oxychloride immediately to generate acridine derivatives **3**. At last, chloroacridines **3** reacted with NH_2-L-NH_2 to give the target compounds **A1-A4**.

2.3. Procedure of intermediate 2-3

The intermediate 2–3 were prepared according to previous reports.[3,4,23]

2.4. General procedure of acridine derivatives A1-A4

The reaction mixture of intermediates **3** (0.42 mmol, 2.05 equiv), phenol (2 mL), alkylamines (NH_2-L-NH_2, 0.2 mM) was stirred at 120 °C for 8–12 h, then monitored by TCL. After cooling down, ice-cold ethyl acetate (20 mL) was added and stirred at 0 °C for 5 min, then 25 mL ice-colded 20 % NaOH was added and stirred for 10 min. The organic layer was extracted with ethyl acetate (5 mL × 2), the combined organic phase was washed with 5 % NaOH, then brine, dried over anhydrous sodium sulfate, filtered and concentrated in vacuum and purified by chromatography on silica gel with DCM/MeOH (10/1–5/1, 1 % $NH_3 \cdot H_2O$ contained) to give **A1-A4**.

N^1-(2,7-dimethylacridin-9-yl)-N^2-(2-((2,7-dimethylacridin-9-yl) amino)ethyl)ethane-1,2-diamine (**A1**). Yellow solid, yield 76 %. ^{1}H NMR (400 MHz, DMSO-d_6) δ 8.04 (s, 2H), 7.71 (d, J = 8.5 Hz, 2H), 7.43 (d, J = 8.7 Hz, 2H), 3.82 (t, J = 6.0 Hz, 2H), 2.93 (t, J = 6.1 Hz, 2H), 2.38 (s, 6H). ^{13}C NMR (101 MHz, DMSO-d_6) δ 150.92, 146.87, 132.35, 131.75, 127.97, 122.93, 117.24, 50.26, 49.78, 21.86. Purity was determined to be 94.1 % by using HPLC. HRMS (ESI; *m/z*). Calcd. for $C_{34}H_{35}N5$, $[M + H]^+$, 514.2965; found: 514.2963.

N^1-(2-methylacridin-9-yl)-N^2-(2-((2-methylacridin-9-yl)amino)ethyl) ethane-1,2-diamine (**A2**). Yellow solid, yield 49 %. ^{1}H NMR (400 MHz, $CDCl_3$) δ 8.12 (d, J = 8.7 Hz, 1H), 8.04 (d, J = 8.6 Hz, 1H), 7.96 (d, J = 8.7 Hz, 1H), 7.86 (s, 1H), 7.60 (t, J = 7.6 Hz, 1H), 7.46 (d, J = 8.8 Hz, 1H), 7.29–7.22 (m, 1H), 3.88 (t, J = 5.2 Hz, 2H), 3.04 (t, J = 5.2 Hz, 2H), 2.39 (s, 3H). ^{13}C NMR (101 MHz, $CDCl_3$) δ 150.85, 148.63, 147.63, 133.09, 132.67, 129.63, 129.09, 129.00, 123.17, 122.92, 121.02, 117.36, 117.30, 49.99, 49.71, 22.00. Purity was determined to be 94.5 % by using HPLC. HRMS (ESI; *m/z*). Calcd. for $C_{32}H_{31}N_5$, $[M + H]^+$, 486.2801; found: 486.2818.

N^1,$N^{1'}$-(ethane-1,2-diyl)bis(N^3-(2-methylacridin-9-yl)propane-1,3-diamine) (**A3**). Yellow solid, yield 52 %. ^{1}H NMR (400 MHz, DMSO-d_6) δ 8.35–8.18 (m, 1H), 8.09–7.97 (m, 1H), 7.75–7.67 (m, 2H), 7.57–7.49 (m, 1H), 7.46–7.37 (m, 1H), 7.25–7.16 (m, 1H), 3.87–3.79 (m, 2H), 2.71–2.53 (m, 4H), 2.45 (s, 3H), 1.90–1.71 (m, 2H). ^{13}C NMR (101 MHz, DMSO-d_6) δ 151.35, 132.49, 131.32, 131.28, 129.77, 125.12, 125.10, 123.15, 123.12, 121.91, 121.90, 116.66, 116.62, 49.57, 49.29, 47.89, 30.74, 21.89. Purity was determined to be 99.7 % by using HPLC. HRMS (ESI; *m/z*). Calcd. for $C_{36}H_{40}N_6$, $[M + Na]^+$, 579.2926; found: 579.2922.

N^1,N^3-bis(2-methylacridin-9-yl)propane-1,3-diamine (**A4**). Yellow solid, yield 58 %. ^{1}H NMR (400 MHz, CD_3OD) δ 7.97 (d, J = 8.7 Hz, 1H), 7.63 (s, 1H), 7.58 (d, J = 8.7 Hz, 1H), 7.52 (t, J = 7.9 Hz, 2H), 7.35 (d, J = 8.8 Hz, 1H), 7.10 (dd, J = 8.3, 6.9 Hz, 1H), 4.04 (t, J = 5.9 Hz, 2H), 2.39–2.30 (m, 1H), 2.27 (s, 3H). ^{13}C NMR (101 MHz, CD_3OD) δ 152.95, 145.37, 143.99, 133.21, 132.34, 130.43, 125.03–124.90 (m), 124.69, 123.72, 121.95, 121.30, 114.77, 114.67, 46.46, 31.30, 20.31. Purity was determined to be 94.3 % by using HPLC. HRMS (ESI; m/z). Calcd. for $C_{31}H_{28}N_4$, $[M + H]^+$, 457.2386; found: 457.2398.

2.5. Biochemicals and materials

All oligomers used in this study were purchased from Sangon. Their concentrations were represented as single-stranded concentrations and determined from the absorbance at 260 nm using a Nanodrop 1000 Spectrophotometer (Thermo Fisher Scientific, USA) with the Beer-Lambert Law: A = ε·C·l. Stock solution of **A1-A4** (10 mM) was prepared using DMSO (100 %), which was purchased from Sigma-Aldrich. Further dilutions to working concentrations were carried out with double-distilled deionized water or buffer.

2.6. Fluorescence resonance energy transfer (FRET) melting assay

The procedures of FRET melting assay was carried out according to the previously published references.[3–5] Dual-labeled FPy33T (5′-FAM-TCCCCACCTTCCCCACCCTCCCCACCCTCCCCA -TAMRA-3′) was prepared as 10 μM solution in 1 × BPES buffer. FPu22T (5′-FAM-TGAG GGTGGGTAGGGTGGGTAA-TAMRA-3′) was prepared as 10 μM solution in Tris-HCl buffer. F10T (5′-FAM-dTATAGCTATA-HEG-TATAGCTATA -TAMRA-3′) was prepared as 10 μM solution in Tris-HCl/KCl buffer. HEG linker is [(-CH_2-CH_2-O-)$_6$]. Donor fluorophore 6-carboxyfluorescein was abbreviated as FAM. Acceptor fluorophore 6-carboxytetramethylrhodamine was abbreviated as TAMRA. Dual-labeled DNAs were pre-annealed. A total volume of 20 μL contained 0.2 μM dual labeled oligonucleotide in corresponding buffer, with or without compounds, which was determined with a Roche Light Cycler 2 real-time PCR instrument. The final analysis of the data was calculate using Origin 8.0 (OriginLab Corp.).

2.7. Surface plasmon resonance (SPR) measurement

The procedures of SPR measurement were carried out according to the previously published references.[3–5] For immobilization, all DNA samples were biotin-labeled and attached to a neutravidin-coated GLH sensor chip. 5′-Biotin labeled Py33 DNA was diluted to 1 μM using Py33 running buffer, 5′-biotin labeled Pu22 DNA and 5′-biotin labeled duplex DNA were diluted to 1 μM using Pu22/duplex running buffer. All 5′-biotin labeled DNAs were pre-annealed. The DNA samples were then captured in flow cells. Different **A1-A4** solutions (50, 25, 12.5, 6.25, 3.125, 0 μM) were prepared in the corresponding DNA running buffer on a ProteOn XPR36 protein interaction array system with a flow rate of 25 mL/min for 260 s of the association phase, followed by 300 s of the dissociation phase. The final graphs were obtained by subtracting blank sensorgrams from the Py33, Pu22, or duplex sensorgrams. Data were analyzed with ProteOn manager software.

2.8. CD experiments

The procedures of CD experiment were carried out according to the previously published references.[3–5,24,25] The Py33 or Pu22 DNA were diluted to 1 μM in the absence or presence of compounds in the corresponding DNA buffer (Py33: 1 × BPES buffer, pH 5.5 or 6.8; Pu22: 10 mM Tris-HCl buffer, pH 7.4). Then pre-annealed and stored at 4 °C overnight. Spectra were recorded three times over a wavelength range of 230–350 nm, averaged, smoothed, and baseline corrected to remove the signal contribution from a buffer. The final analysis of the data was carried out using Origin 8.0.

Table 1
Changes of oligomer's melting temperatures determined by using FRET-melting experiment.

Compound	Δ*T*m (°C)[a]		
	FPy33T	FPu22T	F10T
A1	1.7	14.5	1.9
A2	0.9	13.6	1.4
A3	8.7	14.6	4.1
A4	0.8	13.1	2.3
AD06	2.7	6.2	5.2

[a] Δ*T*m=*T*m (DNA + ligand) - *T*m (DNA). The concentrations of FPy33T, FPu22T and F10T were 0.2 μM, and the concentrations of compounds were 1.0 μM. The melting temperature of FPy33T, FPu22T and F10T in the absence of compounds was 53.2 °C, 66.5 °C and 59.1 °C, respectively.

2.9. Cell culture

Human cancer A375, Hela, A549, U2OS, HCT-116, Siha, and HuH7 cell line were purchased from China Center for Type Culture Collection in Wuhan and maintained in RPMI-1640 or DMEM medium supplemented with 10 % fetal calf serum at 37 °C in a humidified atmosphere with 5 % CO_2.

2.10. MTT cytotoxicity assay

The procedures of MTT assay were carried out according to the previously published references. [3–5,24,25] A375, Hela, A549, U2OS, HCT-116, Siha, and HuH7 cells were seeded on 96-well plates (5.0×10^3 per well) and incubated overnight. The cells were incubated in the presence or absence of different concentrations of compounds (50, 10, 2, 0.4, 0.08, 0 μM) for 48 h. After the culture medium was siphoned off, methyl MTT solution (2.5 mg/mL, 20 μL) was added to each well and further incubated for 4 h. DMSO (200 μL) was added to each well. Then the absorbance was recorded at 570 nm. All doses were tested in three times and final IC_{50} values were calculated by using the Graph Pad Prism 6.0.

3. Results and discussion

3.1. Stable ability of the bisacridine derivatives to c-myc G-quadruplex and i-motif

We first generated a FRET-melting assay to evaluate the thermal stability of the bisacridine derivatives to *c-myc* G-quadruplex and i-motif. As shown in Table 1, compared with MonoA acridine **AD06**, bisacridine derivatives **A1**-**A4** with amine chains and two acridine rings could increase the stability to G-quadruplex structure formed by FPu22T with ΔT_m value range 13.1–14.6 °C, suggesting that two acridine rings linked with amine chains could truly increase the thermal stability to *c-myc* G-quadruplexes. However, **A1**, **A2**, and **A4** linked with a short alkyl amine chain, or alkyl chain, showed relatively weak i-motif stabilizing ability (0.8–1.7 °C) incubated with 5-fold excess ligands. While **A3** introduced with a long alkyl amine linker increased the melting temperatures (8.7 °C), suggesting that long alkyl mine chains could be an important factor for *c-myc* i-motif stabilization. And we also found the weak regularity of stability of bisacridine derivatives to hairpin structure. The synthesized bisacridine derivatives showed weak hairpin (F10T) stabilizing ability, with the ΔT_m valued 1.4–4.1 °C, less than **AD06**.

3.2. Binding affinity of the bisacridine derivatives to c-myc G-quadruplex and i-motif

Next, we used SPR assay to research the binding affinities of the synthesized bisacridine derivatives **A1**-**A4** for *c-myc* G-quadruplex and i-motif. The binding constants (short for K_D value) were determined as

Table 2
The binding affinity of bisacridines **A1-A4** to different DNA determined with SPR assay.

Compound	K_D (μM)[a]		
	Py33	Pu22	Duplex
A1	-[a]	5.5	–
A2	8.9	6.6	17.8
A3	5.5	8.6	12.7
A4	34.5	9.3	16.4
AD06	–	–	9.1

[a] No significant binding was found for the addition of up to 50 μM ligand, which might indicate no specific interactions between the ligand and the DNA.

shown in Table 2. Compared with MonoA acridine, **A1**-**A4** with amine side chains and two acridine rings could bind to a G-quadruplex structure. However, compounds **A1**, **A2**, **A4** linked with short alkyl amine chain or alkyl chain, showed relatively weak binding affinity to *c-myc* i-motif. While **A3** introduced with a long amine chain apparently binds to *c-myc* i-motif with K_D value 5.5 μM, suggesting that the long amine chain could be an important factor for *c-myc* i-motif binding. And we also found the regularity of stability of bisacridine derivatives to haripin structure. As listed in Table 2, **A1-A4** inconspicuously bind to hairpin structure (Duplex) with K_D valued >50 μM, 17.8 μM, 12.7 μM, 16.4 μM, respectively, indicating that the synthesized bisacridine derivatives showed weak hairpin stabilizing ability.

3.3. Interactions of the bisacridine derivatives to c-myc G-quadruplex and i-motif

CD spectroscopy was used usually to determine the conformation of G-quadruplex/i-motif and the interaction between ligands and DNA as well as the formation of other DNA second structures in different conditions.[16,26] Firstly, we study the effects of ligands binding to G-quadruplex. As shown in Fig. 2A, a positive peak at 260–265 nm and a negative peak at near 240 nm indicated Pu22 sequence formed a typical parallel G-quadruplex structure under the condition of 100 mM KCl. While in the absence of potassium ion, the CD spectrum of Pu22 is similar to that in the presence of KCl, but the CD intensity is much lower. After being treated with **A1**-**A4** without metal ion, **A1**-**A4** increased the Pu22 G-quadruplex CD intensity (Fig. 2A). Then we research the effects between *c-myc* i-motif and bisacridines **A1**-**A4**. Py33 showed a positive peak at 287–290 nm and a negative peak at 255–260 nm at pH 5.5, indicating the formation of i-motif (Fig. 2B)[16, 18, 26]. After **A1-A4** were added, the positive peak at 288 nm and negative peak at 260 nm decreased slightly (Fig. 2B), indicating that these compounds could still maintain *c-myc* i-motif conformation.

3.4. Bisacridine derivatives inhibited various carcinoma cells proliferation

We employed the MTT assay to evaluate the cytotoxicity activity of the bisacridine derivatives on various human cancer cell lines. The cytotoxicity activity of **A1-A4** was determined with their IC_{50} values and shown in Table 3. Most of the bisacridine derivatives showed diverse cytotoxicity activity against various tumor cells. The activity of inhibiting tumor cell growth was well consistent with that for inhibition of the ability to bind and stabilize G-quadruplex. Moreover, we found that compound **A3** interacting with G-quadruplex and i-motif, showed a stronger inhibition of the proliferation of tumor cells than these compounds that interacted only with G-quadruplex, such as compounds **A1**, **A2**, and **A4**.

3.5. Binding mode exploration by using molecular modeling

Molecular docking studies were performed to get the molecular modeling using the MOE program. **A3** was docked to the *c-myc* G-quadruplex (PDB ID: 2L7V) and i-motif DNA (PDB ID: 1YBL), respectively. As shown in Fig. 3A and C, the docking results of **A3** with *c-myc* G-quadruplex showed that an acridine ring could effectively stack on the external G-quartet of *c-myc* G-quadruplex, and another acridine backbone could be directed into the DNA grooves and filled the groove space. The

Table 3
The IC_{50} (μM) values of bisacridine derivatives **A1-A4** against different cell lines as determined by using MTT assay.

Comp.	IC_{50} (μM)						
	A375	Hela	A549	U2OS	HCT116	Siha	HuH7
A1	8.97 ± 1.65	13.40 ± 2.39	9.59 ± 1.89	10.11 ± 1.17	10.81 ± 2.12	5.24 ± 1.12	10.27 ± 2.61
A2	9.12 ± 1.97	14.80 ± 4.11	11.72 ± 1.57	6.20 ± 0.85	10.11 ± 3.44	10.96 ± 1.85	11.14 ± 1.58
A3	0.36 ± 0.10	0.55 ± 0.16	0.59 ± 0.10	0.59 ± 0.13	0.51 ± 0.19	0.32 ± 0.06	0.17 ± 0.10
A4	1.50 ± 0.27	3.26 ± 1.13	5.25 ± 0.13	2.61 ± 1.45	4.78 ± 1.15	0.25 ± 0.11	5.51 ± 2.50

The IC_{50} values are represented by the mean ± standard deviation.

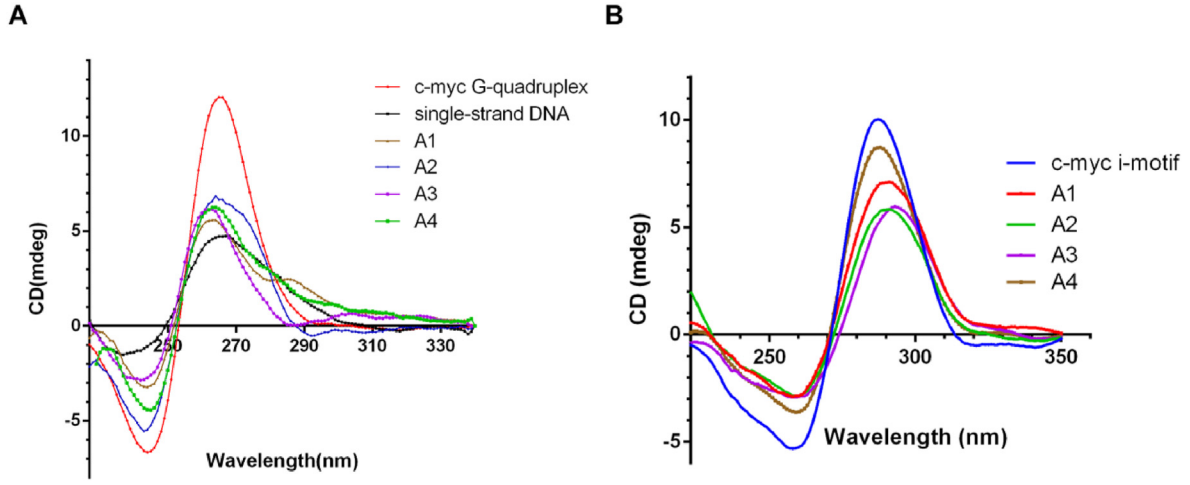

Fig. 2. Interactions of the bisacridine derivatives **A1**-**A4** with *c-myc* promoter G-quadruplex and i-motif. (A) CD spectra of Pu22 in 10 mM Tris-HCl buffer (pH 7.4) in the absence or presence of **A1**-**A4**. (B) CD spectra of Py33 in the absence or presence of **A1**-**A4** at pH 5.5.

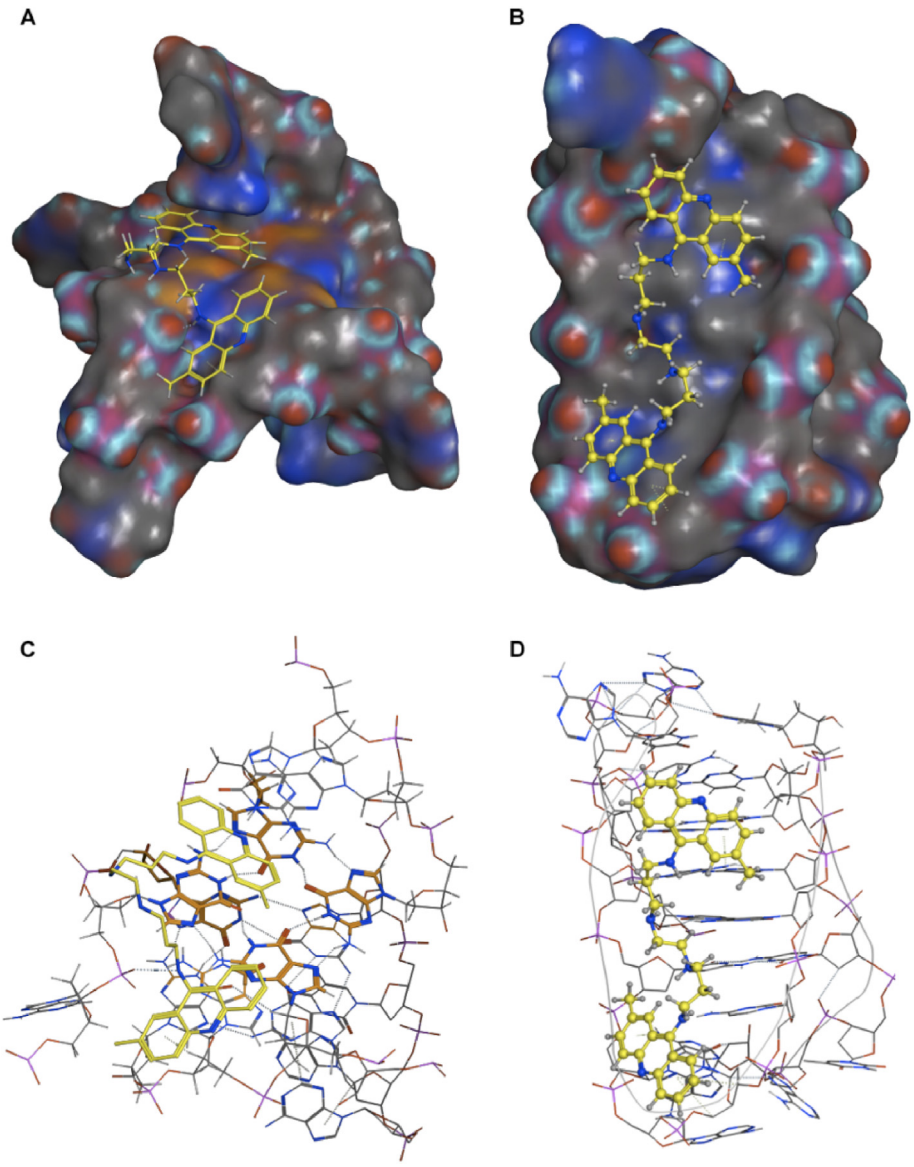

Fig. 3. Molecular docking mode of **A3** (marked with yellow) to *c-myc* promoter DNA secondary structures. (A, C) binding of **A3** to the 5′ end of *c-myc* promoter G-quadruplex (PDB ID: 2L7V); (B, D) binding of **A3** to a model i-motif (PDB ID: 1YBL).

positively charged compound was suitable for the negatively charged phosphate diester backbone of *c-myc* G-quadruplex and formed electrostatic interactions. From Fig. 3B and D, the binding mode uncovered the interaction with i-motif. Just like the binding mode of **A3** with *c-myc* G-quadruplex, not only were the two backbones stacked to loops of the i-motif structure, but there were electrostatic interactions with the grooves. These results further reinforced our design idea that the dimer-acridine might interact with the G-quadruplex and i-motif.

4. Conclusion

In this study, we explored a new strategy for *c-myc* gene transcription inhibition by synthesizing 4 new disubstituted bisacridine derivatives to target the oncogenic *c-myc* promoter G-quadruplex/i-motif. The results of FRET, SPR, and CD experiments indicated that the different disubstituted derivatives with the varying side chain length and amino groups exhibited distinct response to stabilization abilities and binding affinities for *c-myc* G-quadruplex/i-motif. Molecular docking results demonstrated the interaction of **A3** to *c-myc* G-quadruplex/i-motif. In addition, our cellular MTT experiments showed that **A3** exhibited proliferative inhibition effect in cancer cells. These results could help us to found more strong dual G-quadruplex/i-motif binding ligands for further improvement.

CRediT authorship contribution statement

Bing Shu: Methodology, Investigation, Data curation. **Wang-liang Chen:** Methodology, Data curation. **Jia-lin Song:** Formal analysis, Data curation. **Shen Fang:** Writing – review & editing, Writing – original draft. **Jiong-bang Li:** Writing – review & editing, Writing – original draft. **Shang-shi Zhang:** Writing – review & editing, Software.

Declaration of interest statement

The authors declare that they have no known competing financial interests or personal relationships that could have appeared to influence the work reported in this paper.

Acknowledgments

This work was supported by the National Natural Science Foundation of China (Grant: 22007018), the Guangdong Basic and Applied Basic Research Foundation (Grant: 2021A1515011530), Guangdong Provincial Education Department Fund (Grant: 2023ZDZX2028), the Guangzhou Basic and Applied Basic Research Foundation (Grant: 2023A04J) and Medical Science and Technology Research Fund of Guangdong Province (Grant: A2022083).

References

1. Honarpisheh P, Parker SL, Conner CR, et al. 20-year inflation-adjusted medicare reimbursements (years: 2000-2020) for common lumbar and cervical degenerative disc disease procedures. *Global Spine J*. 2024;14(1):211–218.
2. Sung H, Ferlay J, Siegel RL, et al. Global cancer statistics 2020: globocan estimates of incidence and mortality worldwide for 36 cancers in 185 countries. *CA A Cancer J Clin*. 2021;71(3):209–249.
3. Zeng DY, Kuang GT, Wang SK, et al. Discovery of novel 11-triazole substituted benzofuro[3,2-b]quinolone derivatives as c-myc G-quadruplex specific stabilizers via click chemistry. *J Med Chem*. 2017;60(13):5407–5423.
4. Wang YQ, Huang ZL, Chen SB, et al. Design, synthesis, and evaluation of new selective nm23-h2 binders as c-myc transcription inhibitors via disruption of the NM23-H2/G-quadruplex interaction. *J Med Chem*. 2017;60(16):6924–6941.
5. Shan C, Yan JW, Wang YQ, et al. Design, synthesis, and evaluation of isaindigotone derivatives to downregulate c-myc transcription via disrupting the interaction of NM23-H2 with G-quadruplex. *J Med Chem*. 2017;60(4):1292–1308.
6. Lin CY, Loven J, Rahl PB, et al. Transcriptional amplification in tumor cells with elevated c-myc. *Cell*. 2012;151(1):56–67.
7. Cui FM, Sun XJ, Huang CC, et al. Inhibition of c-myc expression accounts for an increase in the number of multinucleated cells in human cervical epithelial cells. *Oncol Lett*. 2017;14(3):2878–2886.
8. Hsu TY, Simon LM, Neill NJ, et al. The spliceosome is a therapeutic vulnerability in myc-driven cancer. *Nature*. 2015;525(7569):384–388.
9. Kaiser CE, Van Ert NA, Agrawal P, et al. Insight into the complexity of the i-motif and G-quadruplex DNA structures formed in the kras promoter and subsequent drug-induced gene repression. *J Am Chem Soc*. 2017;139(25):8522–8536.
10. Kang HJ, Kendrick S, Hecht SM, et al. The transcriptional complex between the bcl2 i-motif and hnrnp ll is a molecular switch for control of gene expression that can be modulated by small molecules. *J Am Chem Soc*. 2014;136(11):4172–4185.
11. King JJ, Irving KL, Evans CW, et al. DNA G-quadruplex and i-motif structure formation is interdependent in human cells. *J Am Chem Soc*. 2020;142(49):20600–20604.
12. Chambers VS, Marsico G, Boutell JM, et al. High-throughput sequencing of DNA G-quadruplex structures in the human genome. *Nat Biotechnol*. 2015;33(8):877–881.
13. Hansel-Hertsch R, Beraldi D, Lensing SV, et al. G-quadruplex structures mark human regulatory chromatin. *Nat Genet*. 2016;48(10):1267–1272.
14. Chambers VS, Marsico G, Boutell JM, et al. High-throughput sequencing of DNA G-quadruplex structures in the human genome. *Nat Biotechnol*. 2015;33(8):877–889.
15. Liu L, Kim BG, Feroze U, et al. Probing the ionic atmosphere and hydration of the c-myc i-motif. *J Am Chem Soc*. 2018;140(6):2229–2238.
16. Wright EP, Day HA, Ibrahim AM, et al. Mitoxantrone and analogues bind and stabilize i-motif forming DNA sequences. *Sci Rep*. 2016;6:39456–39462.
17. Zeraati M, Langley DB, Schofield P, et al. I-motif DNA structures are formed in the nuclei of human cells. *Nat Chem*. 2018;10(6):631–637.
18. Kendrick S, Kang HJ, Alam MP, et al. The dynamic character of the bcl2 promoter i-motif provides a mechanism for modulation of gene expression by compounds that bind selectively to the alternative DNA hairpin structure. *J Am Chem Soc*. 2014;136(11):4161–4171.
19. Qin T, Liu K, Song D, et al. Porphyrin bound to i-motifs: intercalation versus external groove binding. *Chem Asian J*. 2017;12(13):1578–1586.
20. Brown RV, Wang T, Chappeta VR, et al. The consequences of overlapping g-quadruplexes and i-motifs in the platelet-derived growth factor receptor beta core promoter nuclease hypersensitive element can explain the unexpected effects of mutations and provide opportunities for selective targeting of both structures by small molecules to downregulate gene expression. *J Am Chem Soc*. 2017;139(22):7456–7475.
21. Mahajan AA, Rane RA, Amritkar AA, et al. Synthesis of novel amides based on acridone scaffold with interesting antineoplastic activity. *Anti Cancer Agents Med Chem*. 2015;15(5):555–564.
22. Alberti P, Ren J, Teulade-Fichou MP, et al. Interaction of an acridine dimer with DNA quadruplex structures. *J Biomol Struct Dyn*. 2001;19(3):505–513.
23. Kuang G, Zhang M, Kang S, et al. Syntheses and evaluation of new bisacridine derivatives for dual binding of g-quadruplex and i-motif in regulating oncogene c-myc expression. *J Med Chem*. 2020;63(17):9136–9153.
24. Guo QL, Su HF, Wang N, et al. Synthesis and evaluation of 7-substituted-5,6-dihydrobenzo[c]acridine derivatives as new c-kit promoter G-quadruplex binding ligands. *Eur J Med Chem*. 2017;130:458–471.
25. Wang Peng, Sun Zhi-Yin, et al. Design, synthesis, and evaluation of novel p-(methylthio)styryl substituted quindoline derivatives as neuroblastoma ras (nras) repressors via specific stabilizing the rna G-quadruplex. *J Med Chem*. 2018;61(15):6629–6646.
26. Cui J, Waltman P, Le VH, et al. The effect of molecular crowding on the stability of human c-myc promoter sequence i-motif at neutral ph. *Molecules*. 2013;18(10):12751–12767.